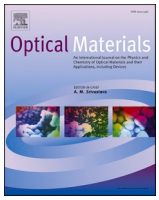
Optical Materials 123 (2022) 111921



Contents lists available at ScienceDirect

Optical Materials

journal homepage: www.elsevier.com/locate/optmat





Role of Al in engineering the optical band gap and PL emission intensity properties of CdO thin films grown by SILAR method

Harun Güney [a], Demet İskenderoğlu [b], Muhammed Emin Güldüren [c,*], Sibel Morkoç Karadeniz [d]

[a] Hınıs Vocational School, Department of Medical Services and Techniques, Atatürk University, Erzurum, Turkey
[b] Kazım Karabekir Education Faculty, Department of Science Education, Atatürk University, Erzurum, Turkey
[c] Vocational School, Department of Electric and Energy, Ağrı İbrahim Çeçen University, Ağrı, Turkey
[d] Department of Physics, Art & Science Faculty, Erzincan Binali Yıldırım University, 24100, Erzincan, Turkey

ARTICLE INFO

Keywords:
Al doped CdO Thin films
XRD
SILAR
Bandgap and PL emission Intensity tuning

ABSTRACT

Herein, we report on synthesizing pure and aluminum (Al) doped cadmium oxide (CdO) thin films onto glass slides by successive ionic layer adsorption and reaction (SILAR) method. The optical, electrical, structural, and morphological evaluations were conducted for the produced samples after the grown thin films heat treated in a convection ashing furnace at 200 °C. X-ray diffraction (XRD) results disclosed that the prepared samples posses the polycrystalline cubic phase of CdO material and the (1 1 1) plane was the preferred growth orientation. Besides, the XRD analysis strongly suggested that the integration of aluminum into the CdO lattices completed as no other phases, such as Cd, Al, or related oxides, were present in the diffraction patterns. From the field emission scanning electron microscope (FE-SEM) images, it was noticed that Al doping concentration changed the surface morphologies. Energy dispersive X-ray analysis (EDAX) confidently proves the presence of Al as a result of the SILAR process. The optical properties were assessed by performing Ultraviolet–visible spectroscopy (Uv–vis), and it was observed that the optical bandgap increased from 2.5 eV to 3 eV due to the increased percentages of Al content in the Al:CdO nanostructures. The Photoluminescence (PL) spectrum evidently showed that the PL emission intensity of prepared samples was directly influenced over varying Al content in the CdO nanostructures. The electrical features of the SILAR derived CdO thin films uncovered that the resistivity of samples showed increment with the Al doping, thus the electrical conductivity of the grown samples decreased in return.

1. Introduction

Nanosized metal oxide thin films have gained researchers attention on the accounts of their wide-ranging implementations in gas sensors, solar cells, photovoltaic devices, transparent electrodes, flat panel displays and so forth [1–6]. In particular, transparent conducting oxides (TCOs) zinc oxide (ZnO), indium oxide (In_2O_3), tin dioxide (SnO_2), cadmium oxide (CdO), etc. are considered quite outstanding semiconductors thanks to being highly transparent in the visible spectrum, and having low resistivity [7–9]. Cadmium oxide is one of the most significant TCO material by being an n type semiconductor with a cubic crystal structure (face center cubic (fcc) type, and lattice constant a = 4.695 Å), having high carrier mobility, and a narrow direct bandgap of 2.2–2.5 eV [5,10–12]. CdO thin films are utilized in a broad spectrum of applications like photodiodes, display technologies, gas sensors, optical communications, photovoltaics, phototransistor, catalysis, and water treatment etc. [12–23]. Furthermore, it is known that the physical properties of CdO nanocrystals can be manipulated to improve its optoelectronic device performance by introducing Al [1], Mn [2], La [3], Cr [4], Ga [9,19], Zn [18], Y [24], Sn [25], Sc [26], Eu [27] etc., which could enhance its n-type conductivity and alter its bandgap.

Various techniques have been put to use for growing CdO thin film samples, such as spray pyrolysis [1,18], microemulsion method [6], sol–gel method [19], pulsed laser deposition [20–23], DC-RF magnetron sputtering [8], chemical bath deposition [15], hydrothermal method [11,16], thermal evaporation [27,28], e-beam evaporation technique [12] and successive ionic layer adsorption and reaction (SILAR) [10,29]. Within these thin film growth methods, SILAR has many advantages due to being low cost, user friendly, and reproducible as well as it enables even coating of large substrate area without any sophisticated vacuum or heating element [5,10]. Although, many studies have been executed on the CdO semiconductor thin films, the reports on the synthesis of Al

* Corresponding author.
E-mail address: megulduren@agri.edu.tr (M.E. Güldüren).

https://doi.org/10.1016/j.optmat.2021.111921
Received 24 November 2021; Received in revised form 15 December 2021; Accepted 16 December 2021
Available online 21 December 2021
0925-3467/© 2021 Elsevier B.V. All rights reserved.

doped CdO thin films by SILAR method are very scarce or non-existent in the literature. Currently, in the web of science database, there are 14 studies which include "Al doped CdO" as keywords in their title, however, none of these works employed the SILAR method to grow their thin films.

In the present work, we present the deposition of pure and Al doped CdO thin films by performing the SILAR method as it is simple, repeatable and economic. Also, the optical, structural, morphological, and electrical (I–V) properties of grown CdO and Al:CdO nanostructures were analyzed by using the Uv–vis spectrometer, XRD, FE-SEM, Photoluminescence and Iviumstat since finding a complete work regarding the effects of Al doping on CdO nanostructures is very limited. And, to our best knowledge, this will be the first study that divulges on the SILAR deposition of CdO thin films doped with aluminum atoms.

2. Experimental

The pure CdO and Al doped CdO thin films were grown on glass slides by the SILAR method. Before beginning the deposition procedure, the glass slides ought to be cleaned in order to prevent any surface contaminants which can hinder the formation of good quality thin film structures. Firstly, the glass substrates were cleaned with diluted (by 1/5 ratio) sulphuric acid in an ultrasonic bath for 300 s. Then, the slides were rinsed using deionized (DI) water in the ultrasonic bath for another 300 s to finish the decontamination process. Fig. 1 demonstrates the schematic representation of one complete period of SILAR cycle. A cationic solution was made from 0.1 M of cadmium nitrate, and variable dopant concentrations of 0.1 M aluminum nitrate. These materials were purchased from Sigma–Aldrich Co. These doping ratios were 1% (CAO1), 2% (CAO2), and 4% (CAO3), respectively. Also, an anionic precursor was formed by using DI water in which pH level adjusted to 11.2 by ammonium hydroxide (29%) solution. Then, as shown in Fig. 1, a computer software operated mechanical system was set up to carry out the demanded number of cycles where the glass slides were first dipped into the cationic solution for 30 s, then followed by submerging into the anionic solution for another 30 s. After 20 cycles of coating performed by the SILAR method at room temperature, the produced samples were annealed at 200 °C for 3600 s to complete the fabrication of these specific CdO thin films. .

3. Results and discussions

Fig. 2 shows the XRD patterns of the pure and Al doped CdO thin films where the Bragg diffraction angles (2θ) were varied in the range of 20° to 70°. There are two major peaks which are distinctly observed in Fig. 2. These peaks are in the planes of (1 1 1) and (2 0 0) which are located at 2θ values of 33.05° and 38.40° for pure CdO sample. These peaks can be observed for all the CdO thin films, and they can be found at almost same 2θ positions as displayed in Table 1. However, the (2 2 0) plane (2θ = 55.35°) appears very softly for pure CdO sample, and it is the most visible in the plotted XRD pattern CAO2 nanostructures. These occurrences may reflect the formation of polycrystalline CdO thin film samples. And, all these XRD findings are in accordance with ICSD standard card number 03-065-2908 confirming the formation of cubic CdO crystals with Fm3m space group [30]. In addition to that, there are no other phases detected on the XRD spectrum that could be related to Al and Cd or their possible oxides. Therefore, it is safe to state that aluminum ions have successfully been integrated into the CdO crystal lattices by performing SILAR method. Moreover, the peak intensities for the planes of (1 1 1), (2 0 0) increased strongly while the aluminum doping concentration rose to 2% as shown in Fig. 2. And, the other weak intensity peak for (2 2 0) was also displayed more clearly in the XRD figure of CAO2. Thus, one may claim that the changed crystallinity of CdO nanostructures can lead to these structural modifications in the XRD spectra due to the Al dopings [5,10]. On the other hand, it is also well known that the internal stress, caused by owning different ion sizes between Al^{3+}(118 pm) and Cd^{2+}(97pm), may also come into play during the deposition process, which might change the balance in energy levels among separate crystal plane orientations. Therefore, it is thought that this phenomenon can be hold responsible for the lessening or fading intensities of the given planes in the XRD spectrums [9,29,31].

The interplanar distance (*d*) values of the pure CdO and Al:CdO nanostructures were determined by performing the Bragg's law [18] given below;

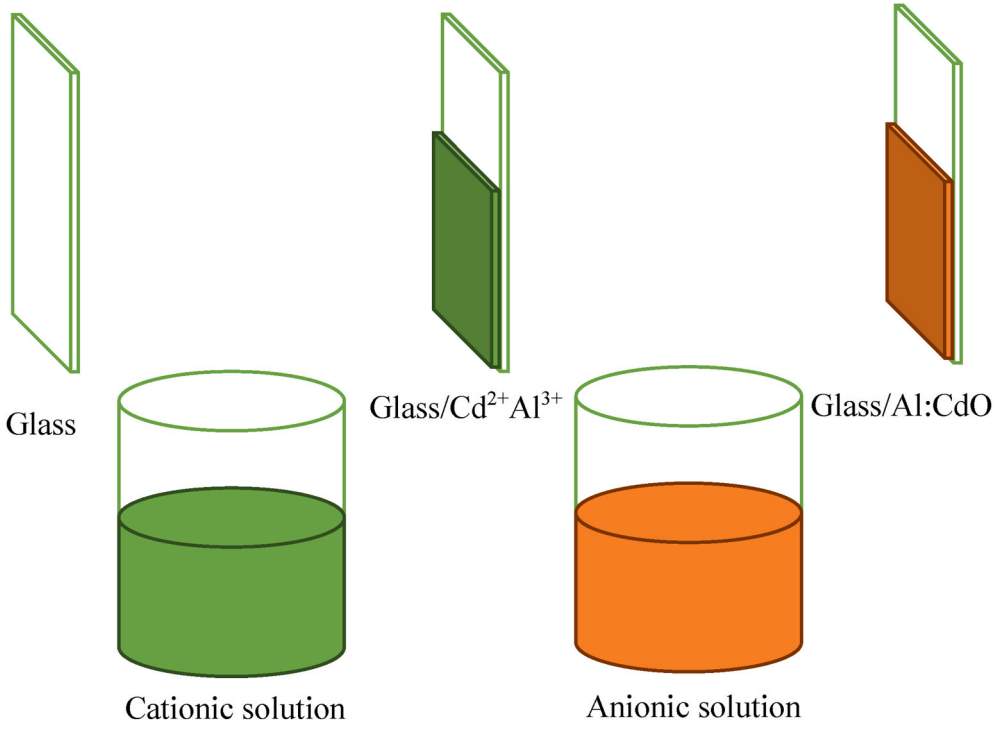


Fig. 1. The SILAR method.

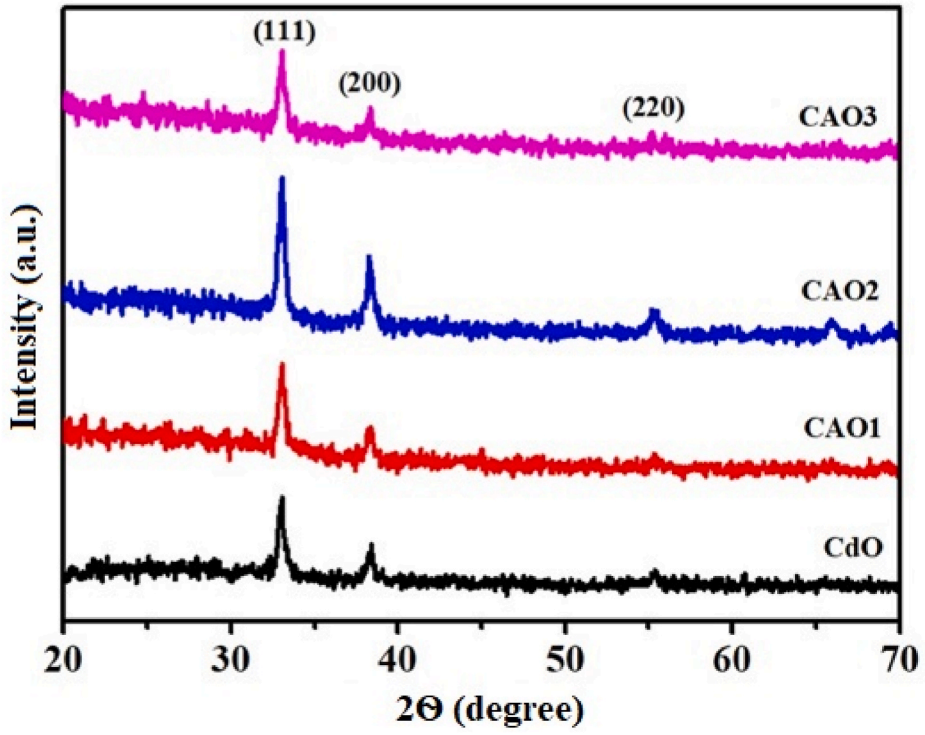


Fig. 2. X-ray diffraction patterns of pure CdO and Al:CdO thin film samples.

Table 1
The calculated band gap (*Eg*), the Miller indices (*hkl*), the Bragg diffraction angle (*2θ*), full width at half maximum (FWHM), texture coefficient (*TC(hkl)*), crystallite size (*D*), dislocation density (*δ*), microstrain values (*ε*), standard (d_0) and derived lattice spacing (*d*), lattice constant (*a*), and volume of the unit cell (*V*) values of the undoped and Al doped CdO films.

Sample Name	E_g (eV)	Miller (hkl)	2θ (°)	FWHM	TC (hkl)	D (nm)	δ (10^{12}/cm^2)	ε (10^{-3})	d_0 (Å)	d (Å)	a (Å)^2	a_{avg} (Å)^2	V (Å)^3
		(111)	33.05	0.393	1.62	194	266	7.5	2.712	2.708	4.691		
CdO	2.50	(200)	38.40	0.314	0.86	239	175	13.1	2.349	2.342	4.685	4.689	103.079
		(220)	55.35	0.388	0.52	181	304	11.4	1.661	1.659	4.691		
		(111)	33.05	0.523	1.67	146	472	10.0	2.712	2.708	4.691		
CAO1	3.00	(200)	38.35	0.370	0.72	203	243	16.8	2.349	2.345	4.690	4.692	103.294
		(220)	55.30	0.259	0.61	272	136	7.2	1.661	1.660	4.695		
		(111)	33.04	0.427	1.58	178	315	8.3	2.712	2.709	4.692		
CAO2	2.93	(200)	38.25	1.323	0.89	57	311	71.7	2.349	2.351	4.702	4.700	103.844
		(220)	55.15	0.512	0.53	137	529	12.4	1.661	1.664	4.707		
		(111)	33.05	0.470	1.59	162	381	9.0	2.712	2.708	4.691		
CAO3	2.73	(200)	38.30	0.351	0.72	214	219	17.3	2.349	2.348	4.696	4.697	103.597
		(220)	55.20	0.391	0.68	180	309	9.9	1.661	1.663	4.703		

$$n\lambda = 2d\sin\theta \quad (1)$$

where *n* equals to 1, θ is the diffraction angle, and λ refers to the X-ray radiation (λ = 1.5406). Observed (*d*) and standard (d_0) interplanar distances are listed in Table 1. And, the found d values for the preferred orientation (1 1 1) fit nicely with the standard values listed in the ICSD card. However, it can be noticed that there are very small fluctuations in numbers for the calculated and standard *d* values as well as the *d* values for pure CdO and Al doped CdO thin films. Hence, it is thought that the variation in the interplanar distances may give an indication to the presence of modified crystal structures due to the defects emerged by aluminum doping [32].

Lattice constant (*a*) and unit cell volume (*V*) were also assessed from the XRD data by employing the formulas [12,18] as follows;

$$d = \frac{a}{\sqrt{(h^2 + k^2 + l^2)}} \quad (2)$$

$$V = a^3 \quad (3)$$

In Table 1, the average lattice constant (*a*) values were exhibited as 4.689, 4.692, 4.700 and 4.697 Å for the grown thin films CdO, CAO1, CAO2, and CAO3, respectively. These values of lattice constant are consistent with the standard value of (*a*) for CdO metal oxides in the given ICSD standard card data (a = 4.695 Å). The computed lattice constants for pure CdO and 1% Al doped CdO were slightly smaller than standard value which may be a result of the existing oxygen vacancies or occurred contractions in the CdO lattices [1]. The calculated *V* values for pure CdO, CAO1, CAO2 and CAO3 were found as 103.079 Å^3, 103.294 Å^3, 103.844 Å^3 and 103.597 Å^3, respectively. These *V* values also match well with the previously mentioned ICSD card data for the cubic structure of CdO nanostructures.

Moreover, in Fig. 3, the texture coefficient ($TC_{(hkl)}$) is used to identify the preferred crystal plane orientations. The $TC_{(hkl)}$ of the grown CdO and Al:CdO nanocrystals were worked out from the XRD data by employing the well-known equation [27] as follows;

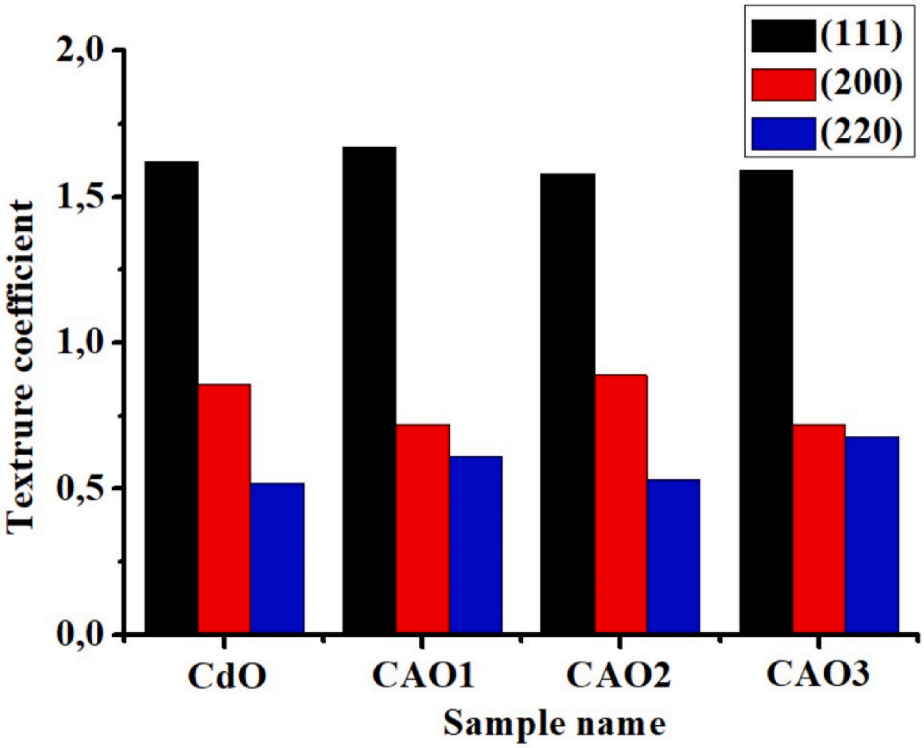


Fig. 3. Variation of *TC* values depending on Al contents in the prepared CdO samples.

$$TC_{hkl} = \frac{I(hkl)/I_0(hkl)}{N^{-1}\Sigma_n I(hkl)/I_0(hkl)} \quad (4)$$

where $I_{(hkl)}$ gives the measured intensity of a plane (*hkl*), $I_{0(hkl)}$ refers to the standard intensity of the (*hkl*) in the related ICSD card data, *N* is the number of reflections, and n symbolize the count of diffraction peaks. For a plane to be considered as preferential orientation, the $TC_{(hkl)}$values would need to be above one [29]. Thus, it can be safely interpreted as the (111) plane was the favorable plane as shown in Table 1, and it prevails over other orientations with increased aluminum content in the cationic precursor. These results are in harmony regarding the previous articles on CdO thin films [5,10,29].

In Fig. 4 and Table 1, the calculated crystallite sizes (*D*) were displayed by performing Debyee Scherrer's formula [9,12,19].

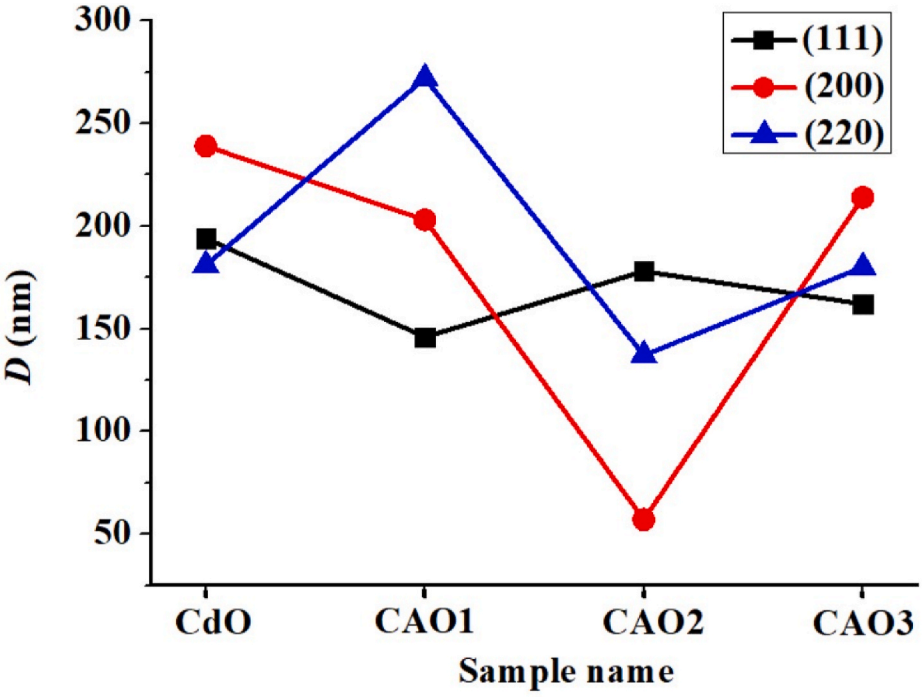


Fig. 4. Variation of crystallite size (*D*) depending on Al contents in the prepared CdO samples.

$$D = \frac{0,9\lambda}{\beta\ cos\theta} \tag{5}$$

where β quantifies the full width at half maximum of the diffraction peak (FWHM), and θ is ascribed to the Bragg's angle. The crystallite (or grain) size for the preferred (111) plane orientation shortened from 194 nm to 146 nm right after the aluminum dopants were introduced to the CdO crystals. Also, the calculated crystal sizes for (2 0 0), and (2 2 0) planes were noted to be ranging from 239 nm to 57 nm and 272 nm–137 nm, respectively. This decrease in the grain size may imply decompositions occurring in the CdO crystallites as given in Table 1 [33]. In addition to that, the observed decrease in the texture factor of (111) plane from 1.62 to 1.58 may also point out to these degradation in the crystalline quality as the doping concentration increased. This degradation may be a result of the high fraction created by doping ions on the surface of crystal boundaries which will increase the internal stress and hinder crystal growth [2].

Table 1 shows the dislocation density *(δ)* and microstrain which was calculated using the given equation below [5,18,19].

$$\delta = \frac{1}{D^2} \tag{6}$$

$$\varepsilon = \frac{\beta\ cos\theta}{4} \tag{7}$$

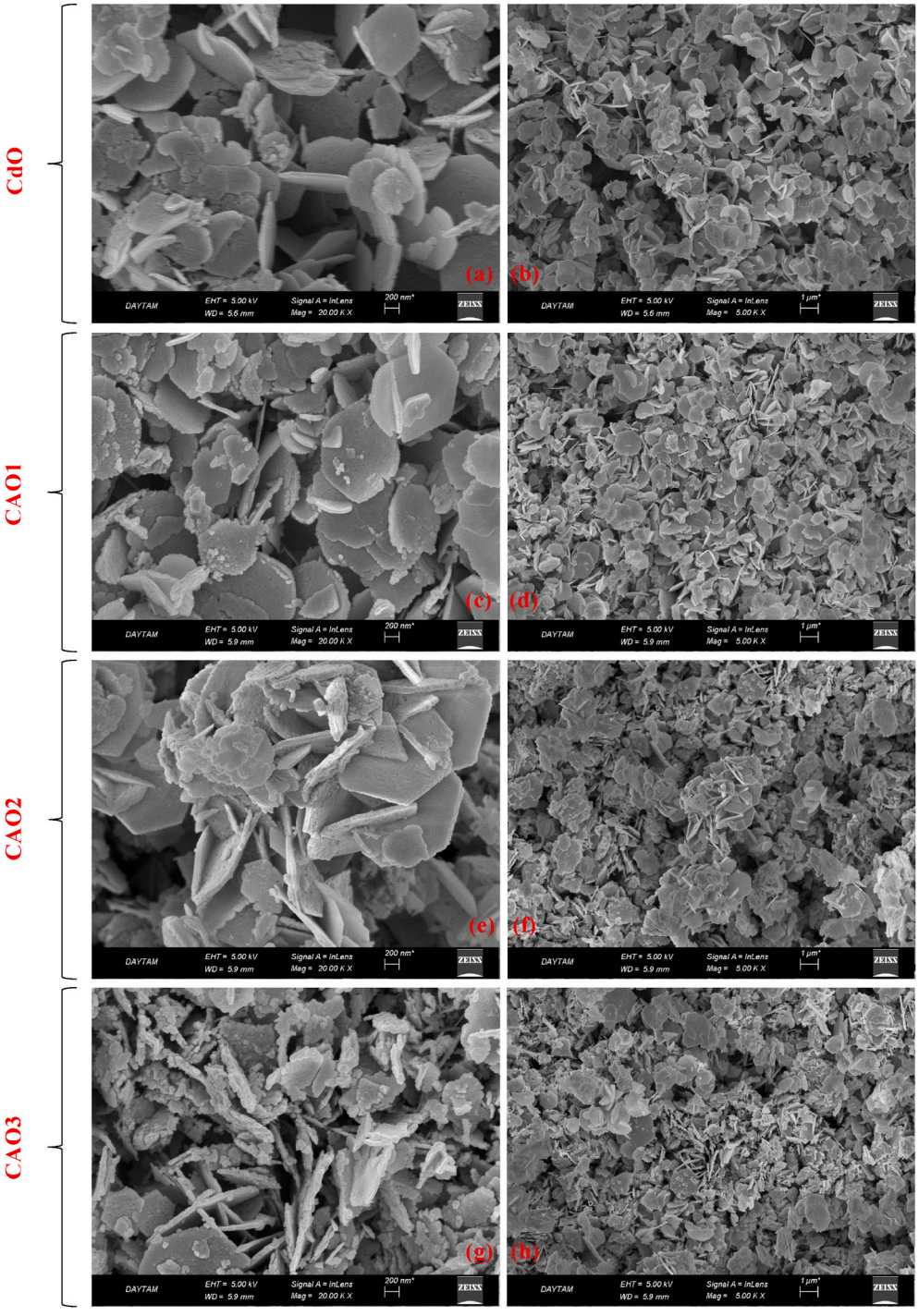


Fig. 5. FE-SEM images of fabricated pure and different concentrations Al doped CdO samples.

It was recorded that the dislocation density for the preferred (111) plane orientation increased from 266 × 10^{12}(cm^{-2}) to 472 × 10^{12} (cm^{-2}) as the Al dopants introduced to the CdO nanostructures. And, for the other two recognized planes orientations, (2 0 0) and (2 2 0), in the XRD analysis shown in Table 1 and Fig. 2, the dislocation densities were found to vary from 175 × 10^{12} (cm^{-2}) to 311 × 10^{12} (cm^{-2}), and 136 × 10^{12} (cm^{-2}) to 529 × 10^{12} (cm^{-2}), respectively. Since this data determines the state of defects in the produced thin films, it confirms the varying numbers of imperfection areas via deposition of different amount of aluminum dopants by SILAR method. Similarly, the microstrain data showed increment from 7.5 × 10^{-3} (cm^{-4}) to 10 × 10^{-3} (cm^{-4}) for the (1 1 1) preferential orientation. And, in general, the obtained microstrain for the other orientations also increased in values displayed in Table 1, while impurity concentration increased.

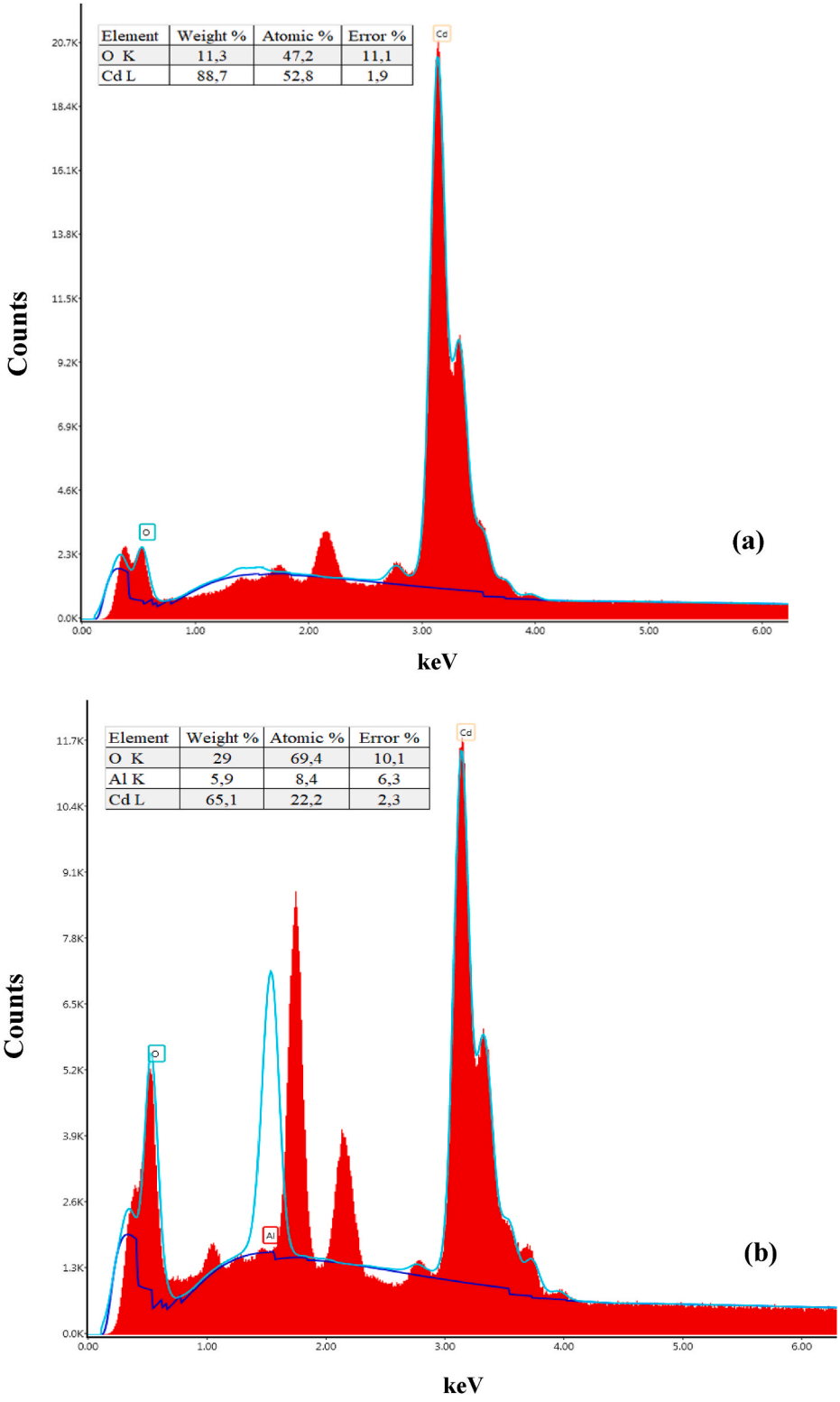


Fig. 6. EDAX spectra with elemental composition of (a) CdO and (b) 4% Al doped CdO thin film.

Furthermore, the polycrystalline nature of prepared CdO samples may enable the alterations in microstrain values as well as the different atomic sizes of Al^{3+} and Cd^{2+} ions [3,28]. The increase in the microstrain and dislocation density data, and the decrease in the crystallite size may imply the existent deteriorations in crystallographic nanostructures of Al:CdO thin films which caused by Al dopings [18,19,33]. The articles published earlier show similar results [1,8,9].

Fig. 5 displays the micro morphological surface structure of synthesized CdO samples which were carried out by Zeiss–Sigma300 FE-SEM. Fig. 5 (a, c, e, g) demonstrate a more close up look into the thin films magnified 20,000times while Fig. 5 (b, d, f, h) cover a more overall perspective of prepared thin films magnified 5000 times. The purpose of taking SEM images is to examine surface properties of produced thin films before and after Al doping, which can be critical for optoelectronic applications. As it can be seen in Fig. 5(a–f), nanosized Al:CdO structures were successfully formed after the SILAR deposition. And, the grown CdO and Al:CdO thin films demonstrate porous nanoflake agglomerates where randomly shaped grain structures can be seen. As discussed in the XRD analysis, the formation of smaller grains in the favored plane orientation was occurred as a result of increase Al doping concentration in CdO nanostructures. Accordingly, these grains shrunk in size may be bonded collectively as a consequence of increment in aluminum doping degrees in the grown CdO samples, thus a more compact accumulation of nanoflake clusters realized [4]. Therefore, the Al dopant can be held accountable for the changes in surface structures of grown CdO crystallites by changing grain size along with the uniformity. In addition to that, EDAX spectrums of the pure CdO and 4% Al doped CdO thin films were also conducted in order to further confirm the targeted elemental occurrences on the glass slides after the effective SILAR depositions of these samples as presented in Fig. 6. The EDAX measurement of 4% Al doped sample was taken next to the pure CdO sample considering it had more compact clusters in SEM images. Thus, it was observed that the fabricated thin films unmistakably contain the Cd, Al, and O materials as verified by the peaks corresponding to the specified elements for the pure CdO and 4% Al doped CdO thin films. This analysis was very significant to witness again how the Al doping impacted the weight and atomic percentages of Cd and O in the CdO crystal structure as these after-effects were also subject of variations in the XRD data given in Table 1.

Fig. 7 shows the impact of aluminum subjects on the optical absorbance spectras of CdO thin film samples. The formation of absorption band edge was observed around 300 nm for the grown nanostructures due to the replacement of Cd with Al atoms in the SILAR grown crystal system of CdO samples. Besides, this cut-off in the absorption spectrum was shifted to lower absorbance levels due to the introduced impurities. This observed variation may be interpreted by the presence of quantum size effects [5]. And, this phenomenon can also be explained as a result of excitations of electrons from valence band to conduction band [7,9,30]. Furthermore, as the aluminum doping density was intensified, the absorption edges blue shifted to shorter wavelengths which may point out the formation of the broadened optical bandgaps as displayed in Table 1. This broadening in the band gap is known as the Moss–Burstein shift [9,23,34].

In Fig. 8, the direct bandgap energies were calculated by applying the Tauc relation [11,19,21,30];

$$\alpha = \frac{Absorbance}{t} \tag{8}$$

$$(\alpha h\upsilon) = A\left(h\upsilon - E_g\right)^n \tag{9}$$

where $h\upsilon$ is the photon energy, α symbolizes the absorption coefficient, t quantifies the thickness, and A refers to an energy-independent constant semiconductor. The bandgap value was found to be 2.5 eV for pure CdO thin films. The obtained band gap for pure CdO is in good agreement with the relevant previous studies [8,18]. In Fig. 8, the bandgap energies were observed to increase simultaneously with the increase of aluminum content in CdO nanocrystallites. This may also be a sign of increased carrier concentrations due to Al ions in the CdO lattice [5,11]. The E_g values are shown in Table 1 as 3eV, 2.93 eV, and 2.73 eV for 1%, 2%, 4% aluminum doped nanostructures, respectively. This increase in bandgap may be caused by the structural improvements, regarding changed crystallite sizes, discussed in the XRD analysis, and displayed in Table 1

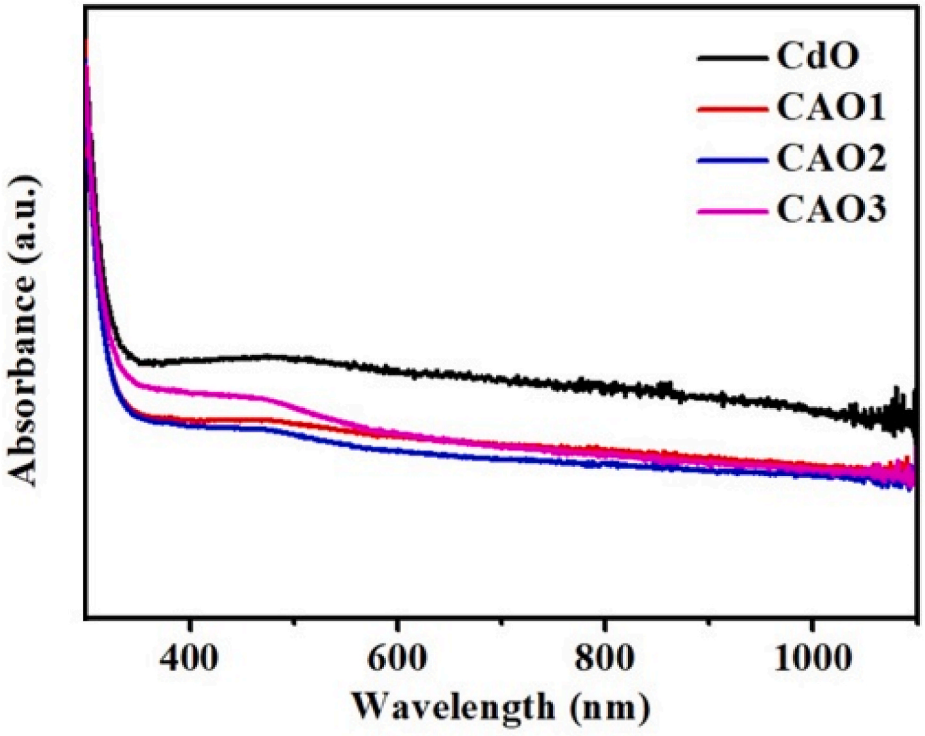


Fig. 7. Absorbance spectra of pure and Al doped CdO thin films.

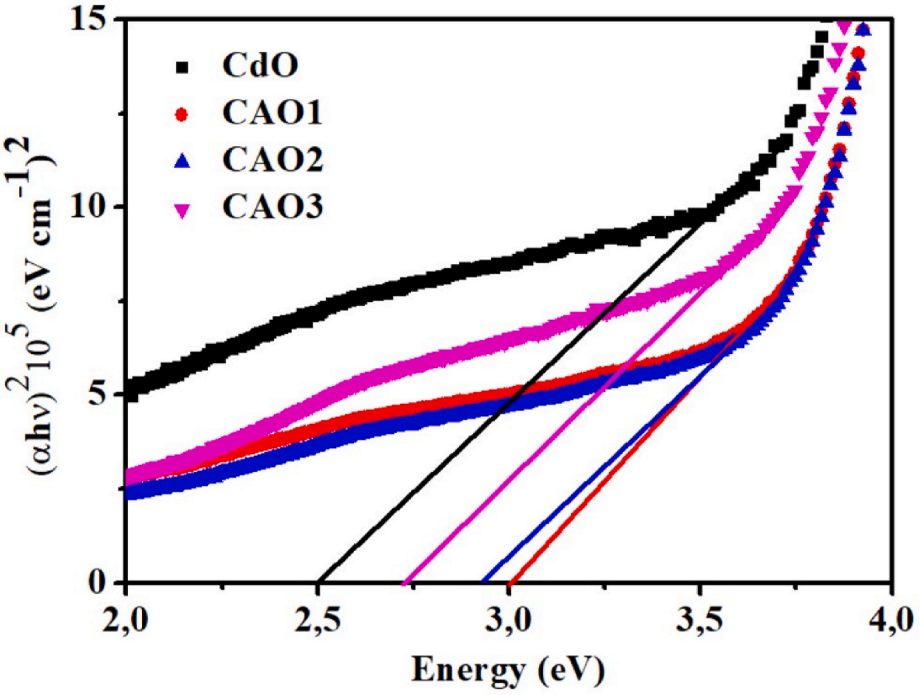


Fig. 8. Bandgap energy variation of CdO nanostructures depending on different Al doping concentrations.

which ultimately leads to modify the optical properties of the prepared cadmium oxide samples [27,30,35]. In addition to that, earlier studies reported similar blue shift behavior in the optical bandgap spectra of doped materials whose dopants possess higher bandgaps than their host [9,28,36]. As the bandgap of bulk Al_2O_3, 6.2 eV at room temperature, is higher than that of the presented pure CdO sample, it can be safe to assume that the bandgap energies of aluminum doped CdO thin films will be produced with bigger optical bandgaps than the pure CdO nanostructures [29,31]. Hence, this could also bring the very likely idea of utilizing the aluminum ions as bandgap regulators for the CdO films to be used in applications such as photovoltaic devices, LCDs, sensors, LEDs, information storage technologies, and so forth [1].

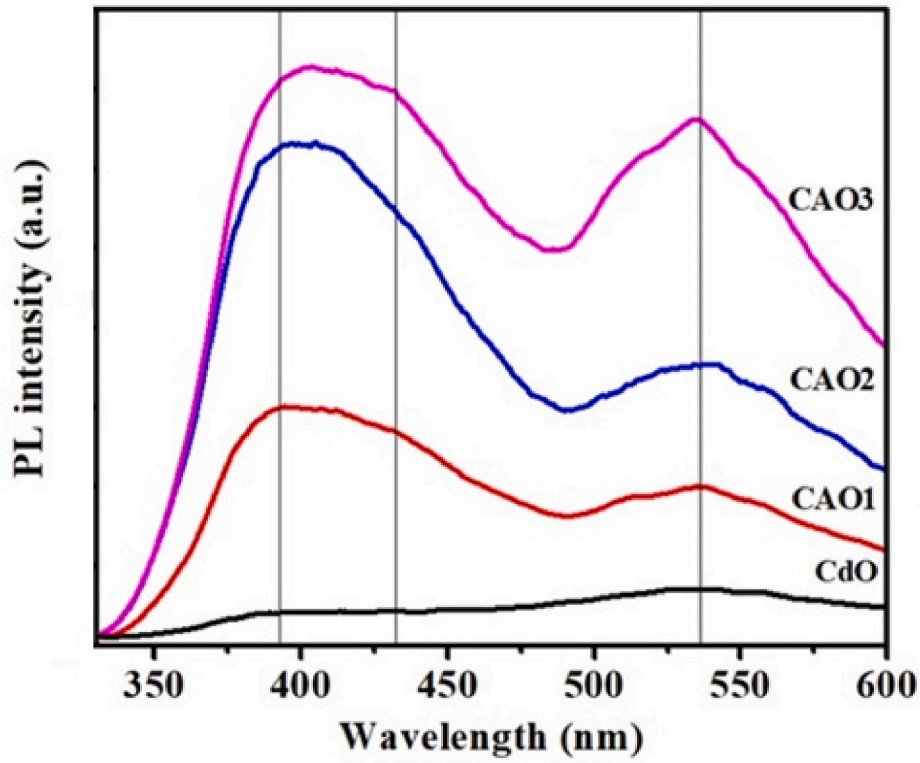


Fig. 9. The PL emission spectra of the pure and Al doped CdO thin films.

Fig. 9 demonstrates the photoluminescence spectra of the synthesized pure CdO and CAO products, which was aimed to help comprehend the impacts of the Al doping on the optoelectronic traits of the CdO thin films. Firstly, it is very clear that the pure CdO nanostructures showed weak luminescence behavior which may be caused by quantum size effect (particle size effect) [5,6]. And, as the Al concentration was increased in the CdO lattices, the intensity of emission peaks were also amplified. Then, there are two distinctive PL peaks as shown in Fig. 9. These emission peaks are located at 395 nm (3.14 eV) and 540 nm (2.29 eV). And, there is also another almost vague peak formed at 436 nm (2.84 eV). These emission peaks can be ascribed to the blue (400–450) and near green (550 nm) emission bands (NGB). Therefore, the blue band and NGB emission intensities enhanced accordingly with the increased Al doping concentration which can release free electrons to the host CdO lattices and thus eliminate vacancy imperfections. This behavior is known as coulomb shielding which has influence on the intensity of green band emissions. The increment in the emission intensities may also indicate the existence of decreased defect sites and oxygen vacancies, known to lead variations in the PL emission intensity as a result of electron-hole pair recombinations [9,20,23,28]. Besides, the reduced deformity can also imply the improved quality and perfection of synthesized Al:CdO crystallites. And, the doping effects, contributed to the changes in the emission intensities, were also mentioned in the XRD data and Uv–vis spectrometry.

Fig. 10 demonstrates the measured I–V characteristics of the pure CdO and different concentration Al:CdO thin film samples. The measured I–V characteristics curves revealed that the current value, corresponding to the applied voltage in the range of +5 to −5 V, of pure CdO decreased after the different aluminum doping levels introduced to the system. And, it was found that the electrical conductivity of the pure CdO sample has the highest electrical conductivity whereas the 1% Al doped CdO sample has the lowest conductivity. These happenings may be justified by the changed crystallinity of CdO samples and surface roughness due to aluminum dopings as shown in the XRD data, and SEM images [37]. Therefore, it can be said that the pure CdO nanocrystals has better electrical conductivity without any extrinsic Al doping which increases the resistance of host structures and causes lower electrical conductivity.

4. Conclusions

In the present study, the SILAR technique was applied to produce the pure and Al doped CdO thin films on the glass slides for the first time according to literature survey. The aftermath of aluminum doping were also investigated in respect of structural, morphological, optical and electrical properties of the prepared CdO nanostructures. In the XRD analysis, it was observed that the grown samples were polycrystalline cubic structures having preferential orientation along (1 1 1) plane. And, it was also see that the crystallite size for the preferred (111) plane orientation decreased from 194 nm to 146 nm due to the doping with aluminum. The FE-SEM images showed that Al doped CdO nanostructures displayed certain morphologic modifications as compared to the nanoflake structure of the pure CdO sample. The EDAX results acknowledged the integration of Al ions in the CdO thin films coated by the cost effective SILAR method. The direct optical bandgap shifted to the higher energy, from 2.5 eV to 3 eV, as a result of the introduction of Al ions to the CdO nanostructures which ultimately amplified the carrier concentration of the grown samples. The PL spectroscopy exhibits emissions at 2 different energies whose intensities were noted to be exactly proportional to the existing Al doping percentages. The electrical (I–V) measurements also illustrated that CdO samples greatly affected by the presence of Al ions which altered the conductivity of prepared samples entirely. Therefore, Al doping can be considered as a tuning agent for the physical assets of CdO thin films which can be beneficial for optoelectronic applications of cadmium oxides such as lasers, solar cells, photodiodes, optical communications, LEDs, smart windows, etc.

CRediT authorship contribution statement

Harun Güney: Conception and design of study, acquisition of data, Formal analysis, Drafting the manuscript, revising the manuscript critically for important intellectual content, Approval of the version of the manuscript to be published. **Demet İskenderoğlu:** Conception and design of study, acquisition of data, Formal analysis, Drafting the

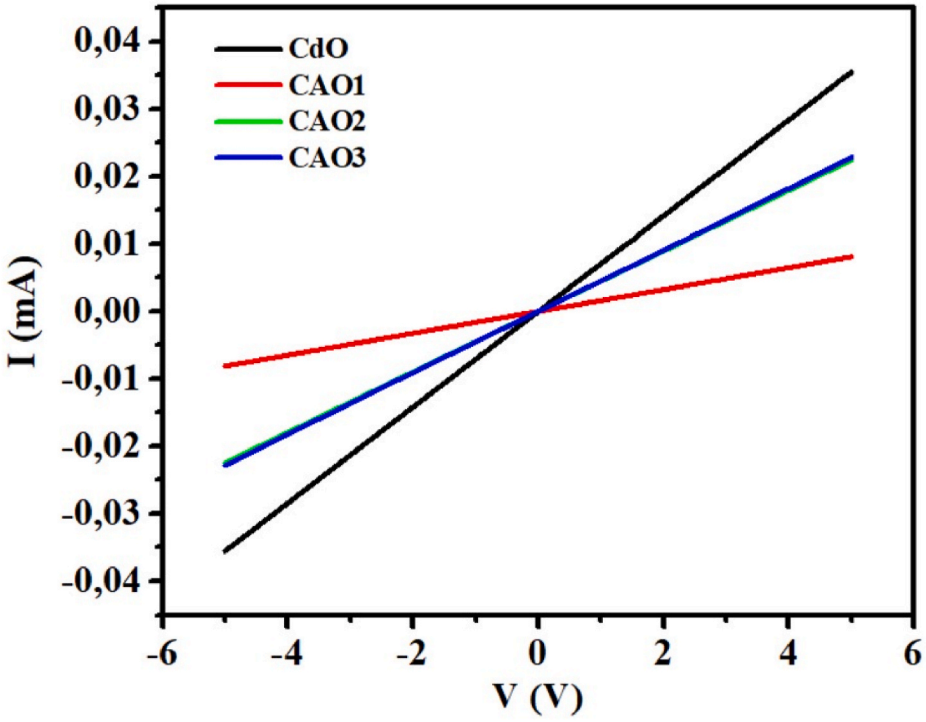


Fig. 10. The I–V characteristics of pure and Al doped CdO thin films.

manuscript, revising the manuscript critically for important intellectual content, Approval of the version of the manuscript to be published. **Muhammed Emin Güldüren:** Conception and design of study, acquisition of data, Formal analysis, Drafting the manuscript, revising the manuscript critically for important intellectual content, Approval of the version of the manuscript to be published. **Sibel Morkoç Karadeniz:** Conception and design of study, acquisition of data, Formal analysis, Drafting the manuscript, revising the manuscript critically for important intellectual content, Approval of the version of the manuscript to be published.

Declaration of competing interest

The authors declare that they have no known competing financial interests or personal relationships that could have appeared to influence the work reported in this paper.

Acknowledgements

The authors did not receive support from any organization for the submitted work.

References

[1] Rahman, Aminur, MdShahjahan, Most Halima Khatun, Structural, optical and electrical properties of Al doped CdO thin films deposited by spray pyrolysis method, IOSR J. Appl. Phys. 11 (6) (2019) 9–14, https://doi.org/10.9790/4861-1106010914.

[2] N. Manjula, M. Pugalenthi, V.S. Nagarethinam, K. Usharani, A.R. Balu, Effect of doping concentration on the structural, morphological, optical and electrical properties of Mn-doped CdO thin films, Mater. Sci. -Poland 33 (4) (2015) 774–781, https://doi.org/10.1515/msp-2015-0115.

[3] P. Velusamy, R. Ramesh Babu, K. Ramamurthi, E. Elangovan, J. Viegas, Effect of La doping on the structural, optical and electrical properties of spray pyrolytically deposited CdO thin films, J. Alloys Compd. 708 (2017) 804–812, https://doi.org/10.1016/j.jallcom.2017.03.032.

[4] B. Hymavathi, B. Rajesh Kumar, T. Subba Rao, Structural, surface morphological and optical properties of Cr doped CdO thin films for optoelectronic devices, Mater. Today Proc. 2 (4–5) (2015) 1510–1517, https://doi.org/10.1016/j.matpr.2015.07.077.

[5] B. Gokul, P. Matheswaran, R. Sathyamoorthy, Influence of annealing on physical properties of CdO thin films prepared by SILAR method, J. Mater. Sci. Technol. 29 (1) (2013) 17–21, https://doi.org/10.1016/j.jmst.2012.11.015.

[6] Wenting Dong, Congshan Zhu, Optical properties of surface-modified CdO nanoparticles, Opt. Mater. 22 (3) (2003) 227–233.

[7] Irshad Ahmad, Inexpensive and quick photocatalytic activity of rare earth (Er, Yb) co-doped ZnO nanoparticles for degradation of methyl orange dye, Separ. Purif. Technol. 227 (2019) 115726, https://doi.org/10.1016/j.seppur.2019.115726.

[8] I.S. Yahia, G.F. Salem, M.S. Abd El-sadek, F. Yakuphanoglu, Optical properties of Al-CdOnano-clusters thin films, Superlattice. Microst. 64 (2013) 178–184, https://doi.org/10.1016/j.spmi.2013.09.024.

[9] R.J. Deokate, S.V. Salunkhe, G.L. Agawane, B.S. Pawar, S.M. Pawar, K.Y. Rajpure, A.V. Moholkar, J.H. Kim, Structural, optical and electrical properties of chemically sprayed nanosized gallium doped CdO thin films, J. Alloys Compd. 496 (1–2) (2010) 357–363, https://doi.org/10.1016/j.jallcom.2010.01.150.

[10] A. Shameem, P. Devendran, V. Siva, M. Raja, S. Asath Bahadur, A. Manikandan, Preparation and characterization studies of nanostructured CdO thin films by SILAR method for photocatalytic applications, J. Inorg. Organomet. Polym. Mater. 27 (3) (2017) 692–699, https://doi.org/10.1007/s10904-017-0512-1.

[11] Yasemin Pepe, Ahmet Karatay, Yusuf Osman Donar, Sınağ Ali, Huseyin Unver, Ayhan Elmali, Tuning the energy bandgap and nonlinear absorption coefficients of CdO nanocomposite films with doping and annealing process, Opt. Mater. 103 (2020) 109880.

[12] Anuradha Purohit, S. Chander, M.S. Dhaka, Impact of annealing on physical properties of e-beam evaporated polycrystalline CdO thin films for optoelectronic applications, Opt. Mater. 66 (2017) 512–518.

[13] Jeevitesh K. Rajput, Trilok K. Pathak, V. Kumar, H.C. Swart, L.P. Purohit, Tailoring and optimization of optical properties of CdO thin films for gas sensing applications, Phys. B Condens. Matter 535 (2018) 314–318, https://doi.org/10.1016/j.physb.2017.08.014.

[14] BestoonAnwer Gozeh, Abdulkerim Karabulut, Cheman Baker Ismael, , Sarwar Ibrahim Saleh, FahrettinYakuphanoglu, Zn-doped CdO effects on the optical, electrical and photoresponse properties of heterojunctions-based photodiodes, J. Alloys Compd. (2021) 159624, https://doi.org/10.1016/j.jallcom.2021.159624.

[15] M. Ocampo, A.M. Fernandez, P.J. Sebastian, Transparent conducting CdO films formed by chemical bath deposition, Semicond. Sci. Technol. 8 (5) (1993) 750. http://iopscience.iop.org/0268-1242/8/5/024.

[16] Ahmad Umar, M.S. Akhtar, M.S. Al-Assiri, A.E. Al-Salami, S.H. Kim, Composite CdO-ZnO hexagonal nanocones: efficient materials for photovoltaic and sensing applications, Ceram. Int. 44 (5) (2018) 5017–5024, https://doi.org/10.1016/j.ceramint.2017.12.098.

[17] Jeevitesh K. Rajput, Trilok K. Pathak, Vinod Kumar, L.P. Purohit, Influence of sol concentration on CdO nanostructure with gas sensing application, Appl. Surf. Sci. 409 (2017) 8–16, https://doi.org/10.1016/j.apsusc.2017.03.019.

[18] Nagaraja, B. S., S. C. Gurumurthy, Raghavendra Bairy, Koduri Ramam, K. Bindu, and Ashok Rao. "A systematic investigation on structural, electrical, linear and nonlinear optical properties of Zn: CdO thin films for optoelectronic applications." Opt. Mater. 122 (2021): 111669.

[19] A.A.A. Farag, A.M. Aboraia, H. Elhosiny Ali, V. Ganesh, H.H. Hegazy, Alexander V. Soldatov, H.Y. Zahran, Yasmin Khairy, I.S. Yahia, Structural investigation and optical enhancement characterization of nanostructured Ga-doped@ CdO/FTO films for photodiode applications, Opt. Mater. 110 (2020) 110458.

[20] Ayman M. Mostafa, A.A. Menazea, Laser-assisted for preparation ZnO/CdO thin film prepared by pulsed laser deposition for catalytic degradation, Radiat. Phys. Chem. 176 (2020) 109020.

[21] Ayman M. Mostafa, Eman A. Mwafy, Synthesis of ZnO/CdO thin film for catalytic degradation of 4-nitrophenol, J. Mol. Struct. 1221 (2020) 128872.

[22] Ayman M. Mostafa, Eman A. Mwafy, Laser-assisted for preparation Ag/CdO nanocomposite thin film: structural and optical study, Opt. Mater. 107 (2020) 110124.

[23] A.A. Menazea, Ayman M. Mostafa, Emad A. Al-Ashkar, Impact of CuO doping on the properties of CdO thin films on the catalytic degradation by using pulsed-Laser deposition technique, Opt. Mater. 100 (2020) 109663.

[24] Yu Yang, Shu Jin, Julia E. Medvedeva, John R. Ireland, Andrew W. Metz, Jun Ni, Mark C. Hersam, Arthur J. Freeman, J. Tobin, Marks. "CdO as the archetypical transparent conducting oxide. Systematics of dopant ionic radius and electronic structure effects on charge transport and band structure, J. Am. Chem. Soc. 127 (24) (2005) 8796–8804, https://doi.org/10.1021/ja051272a.

[25] B.J. Zheng, J.S. Lian, Lei Zhao, Qing Jiang, Optical and electrical properties of Sn-doped CdO thin films obtained by pulse laser deposition, Vacuum 85 (9) (2011) 861–865, https://doi.org/10.1016/j.vacuum.2011.01.002.

[26] Shu Jin, Yu Yang, Julia E. Medvedeva, John R. Ireland, Andrew W. Metz, Jun Ni, Carl R. Kannewurf, Arthur J. Freeman, J. Tobin, Marks. "Dopant ion size and electronic structure effects on transparent conducting oxides. Sc-doped CdO thin films grown by MOCVD, J. Am. Chem. Soc. 126 (42) (2004) 13787–13793, https://doi.org/10.1021/ja0467925.

[27] A.A. Dakhel, Bandgap narrowing in CdO doped with europium, Opt. Mater. 31 (4) (2009) 691–695.

[28] M. Benhaliliba, C.E. Benouis, A. Tiburcio-Silver, F. Yakuphanoglu, A. Avila-Garcia, A. Tavira, R.R. Trujillo, Z. Mouffak, Luminescence and physical properties of copper doped CdO derived nanostructures, J. Lumin. 132 (10) (2012) 2653–2658, https://doi.org/10.1016/j.jlumin.2012.03.044.

[29] R. Aydin, H. Cavusoglu, B. Sahin, Transition metal Mn/Cu co-doped CdO transparent conductive films: effect on structural, morphological and optical characteristics, J. Alloys Compd. 785 (2019) 523–530, https://doi.org/10.1016/j.jallcom.2019.01.221.

[30] Harun Güney, Demet İskenderoğlu, The effect of Zn doping on CdO thin films grown by SILAR method at room temperature, Phys. B Condens. Matter 552 (2019) 119–123.

[31] Arham S. Ahmed, M.L. Singla, Sartaj Tabassum, Alim H. Naqvi, Ameer Azam, Band gap narrowing and fluorescence properties of nickel doped SnO2 nanoparticles, J. Lumin. 131 (1) (2011) 1–6, https://doi.org/10.1016/j.jlumin.2010.07.017.

[32] R. Rai, TrilokiTriloki, B.K. Singh, X-ray diffraction line profile analysis of KBr thin films, Appl. Phys. A 122 (8) (2016) 1–11, https://doi.org/10.1007/s00339-016-0293-3.

[33] Z.Q. Li, C.J. Lu, Z.P. Xia, Y. Zhou, Z. Luo, X-ray diffraction patterns of graphite and turbostratic carbon, Carbon 45 (8) (2007) 1686–1695, https://doi.org/10.1016/j.carbon.2007.03.038.

[34] Bo E. Sernelius, K.-F. Berggren, Z.-C. Jin, Ivar Hamberg, Claes Göran Granqvist, Band-gap tailoring of ZnO by means of heavy Al doping, Phys. Rev. B 37 (1988), https://doi.org/10.1103/PhysRevB.37.10244, 10244-17.

[35] P. Kumbhakar, D. Singh, C.S. Tiwary, A.K. Mitra, Chemical synthesis and visible photoluminescence emission from monodispersed ZnO nanoparticles, Chalcogenide Lett. 5 (12) (2008) 387–394. https://www.researchgate.net/publication/227722665_Chemical_Synthesis_and_Visible_Photoluminescence_Emission_from_Monodispersed_ZnO_Nanoparticles. (Accessed 20 August 2021).

[36] L.R. de León-Gutiérrez, J.J. Cayente-Romero, J.M. Peza-Tapia, E. Barrera-Calva, J. C. Martínez-Flores, M. Ortega-López, Some physical properties of Sn-doped CdO thin films prepared by chemical bath deposition, Mater. Lett. 60 (29–30) (2006) 3866–3870, https://doi.org/10.1016/j.matlet.2006.03.131.

[37] S.K. Shaikh, V.V. Ganbavle, S.I. Inamdar, K.Y. Rajpure, Multifunctional zinc oxide thin films for high-performance UV photodetectors and nitrogen dioxide gas sensors, RSC Adv. 6 (31) (2016) 25641–25650, https://doi.org/10.1039/C6RA01750A.